

RESEARCH ARTICLE

A Scalable Arrangement Method for Aperiodic Array Antennas to Reduce Peak Sidelobe Level

JIAO ZHANG¹, HONGTAO ZHANG¹, XUELEI CHEN², FENGQUAN WU²,
YUFENG LIU¹, AND WENMEI ZHANG¹, (Senior Member, IEEE)

¹School of Physics and Electronic Engineering, Shanxi University, Taiyuan 030006, China

²National Astronomical Observatory, Chinese Academy of Science, Beijing 100101, China

Corresponding author: Jiao Zhang (zhangjiao@sxu.edu.cn)

This work was supported in part by the Chinese Academy of Sciences (CAS) under Grant ZDKYYQ20200008, in part by the CAS Strategic Priority Research Program under Grant XDA15020200, and in part by the National Natural Science Foundation of China under Grant 11974228.

ABSTRACT Peak sidelobe level reduction (PSLR) is crucial in the application of large-scale array antenna, which directly determines the radiation performance of array antenna. We study the PSLR of subarray level aperiodic arrays and propose three array structures: dislocated subarrays with uniform elements (DSUE), uniform subarrays with random elements (USRE), dislocated subarrays with random elements (DSRE). To optimize the dislocation position of subarrays and random position of elements, the improved Bat algorithm (IBA) is applied. To draw the comparison of PSLR effect among these three array structures, we take three size of array antennas from small to large as examples to simulate and calculate the redundancy and peak sidelobe level (PSLL) of them. The results show that DSRE is the optimal array structure by analyzing the dislocation distance of subarray, scanning angle and applicable frequency. The proposed design method is a universal and scalable method, which is of great application value to the design of large-scale aperiodic array antenna.

INDEX TERMS Subarray level aperiodic array, peak sidelobe level reduction, bat algorithm, redundancy.

I. INTRODUCTION

In the design of array antenna, the reduction of PSLL is very important because it will directly affect the power characteristics and anti-interference performance of the system [1]. The PSLL, usually referring to the normalized maximum sidelobe level value, is the secondary lobe level in the radiation pattern. When the PSLL of array antenna is too high, it will affect the main lobe and cause interference and loss to the energy of the whole array antenna. At the same time, its echo will also interfere with the radar system. Therefore, in order to improve the overall performance of array antenna, it is necessary to reduce PSLL.

There are several ways to reduce PSLL in aperiodic array antennas. Elements optimization is the most basic method, which is realized by optimizing each array element

in a completely random way or following some certain pattern. Smolders [2] has shown a concept of random sequential rotation to provide well-controlled sidelobes in a regular periodic array grid, which has similar ability as randomly-spaced array antennas. Lucas [3] has reported a Fermat's spiral based array antenna to suppress secondary radiation lobes, which has similar sidelobe level and bandwidth as those obtained by computationally expensive non-linear optimization methods. The aperiodic weighted array antennas proposed in literature [4] have excellent bandwidth characteristics which can effectively minimize the PSLL. Haupt [5] has used genetic algorithms by encoding parameters containing location information as binary strings, and the array distribution with the lowest maximum relative sidelobe level is obtained after finite iteration optimization. Due to the outstanding characteristics of aperiodic array antenna, such as wide bandwidth, high resolution and wide scanning angle, it has been widely used in satellite

The associate editor coordinating the review of this manuscript and approving it for publication was Giorgio Montisci¹.

communication, remote sensing [6], [7], [8] and medical imaging [9], [10].

Aperiodic array antennas with optimized elements can greatly reduce PSLL, but for large and medium-sized array, the array structure with high degree of freedom makes it difficult to realize wave control and power feeding. An improved idea is to design subarray level aperiodic array antennas [11], [12], [13], [14], which is a compromise between random array and periodic array. For large scale antennas, a group of antennas can be regarded as an element, namely a subarray, and these subarrays can be placed randomly to greatly reduce the difficulty of analysis. Due to the identity of subarray structures, subarray level aperiodic array [11] can reduce the complexity of design and manufacture, and its PSLL ability is comparable to that of random array.

Both literatures [11], [12] designed the aperiodic arrays with the combination of aperiodic subarray (dislocation) and uniform array elements. The subarray was integrated with multi-channel transceiver module with periodic active channel arrangement, which can greatly simplify the manufacturing technology and effectively reduce the highest sidelobe level. Literatures [13], [14] designed the aperiodic arrays, which is combined of aperiodic subarray (rotating) and non-uniform array elements. Kiersten [13] have studied an aperiodic array composed of aperiodic subarrays (rotating) and non-uniform elements, in which the bandwidth capability and the sidelobe level (SLL) of various arrays were characterized by probability, and their capability of low-cost applications was analyzed. The research shows that the array with rotating random subarrays had good antenna characteristics and the feasibility of low-cost manufacturing. Junming [14] have done some further studies on the array antenna with rotating random subarrays, such as, the number of array elements, the density of array elements and the PSLL, and have done some comparisons with those of pure random array and periodic array antenna, such as, the bandwidth, directivity and design calculation complexity, which further highlights the advantages of subarray-level aperiodic array in design and manufacture.

In this paper, we consider a scalable arrangement method for large and medium-sized subarray level aperiodic array antennas, and propose three aperiodic array structures: DSUE, USRE, and DSRE. The array structure is optimized by IBA to reduce PSLL. The characteristics of different arrays are analyzed by redundancy theory. The influences of the number of elements and subarrays, the dislocation distance of subarrays, scanning characteristics and applicable frequency width on PSLL are analyzed. The simulation results show that DSRE not only has the best PSLL effect, but also has lower computational complexity.

The structure of this paper is arranged as follows. Section II describes the structure of subarray level aperiodic array antennas. Section III introduces array synthesis, application details of the IBA and redundancy theory. Section IV analyzes the PSLL effect of the array in terms of the number

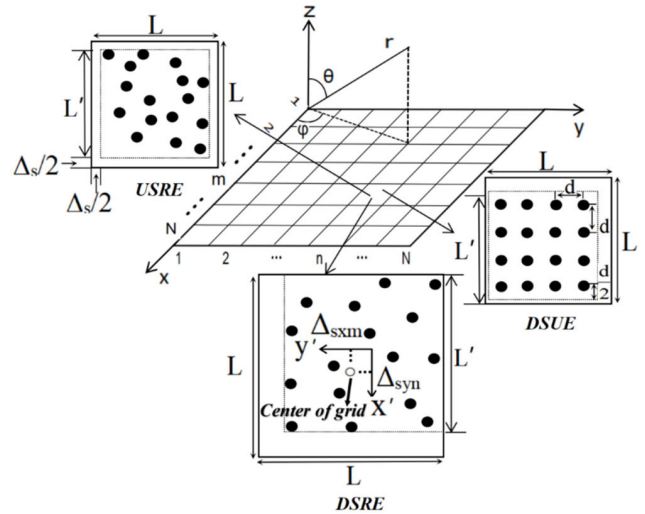


FIGURE 1. Analysis model diagram of three aperiodic array structures with relevant Cartesian (x, y, z) and spherical (r, θ, ϕ) coordinate systems. mn : the subarrays in the m -th row and n -th column; d : element spacing; L' : The size of subarray; L : the size of grid; Δ_s : the longitudinal or transverse dislocation distance of a subarray; Δ_{sxm} and Δ_{syn} : represent the dislocation distance of subarrays in x and y directions respectively.

of elements and subarrays, subarray dislocation distance, scanning characteristics and applicable frequency range. Section V contains the conclusion and discussion.

II. SUBARRAY LEVEL APERIODIC ARRAY DESIGN

We propose three kinds of aperiodic rectangular grid array antennas, each of which is composed of the same subarrays. Fig. 1 is the analysis model diagram of three array structures when the number of elements in the subarray is $M \times M$ (4×4 in the figure) and the number of subarrays is $N \times N$ (7×7 in the figure). The whole array is composed of the same kind of subarrays. Three kinds of array antennas are formed, namely, DSUE, USRE and DSRE. The size of the subarray is L' . The subarray is placed in a square grid with side length L because of the need to vacate the dislocation distance of subarray. The whole array consists of squares grids of the same size which are uniformly and closely arranged, and the distance between the side of subarray and the same side of square grid is $\Delta_s/2$. Δ_s is the longitudinal or transverse dislocation distance of a subarray. There is no strict standard for its value, which needs to be determined according to the designed array. For the array with the average element spacing greater than one wavelength in this paper, generally takes slightly less than one wavelength as the optimal value. The influence of dislocation position is briefly analyzed in the IV section.

Taking 28×28 array elements as an example, Fig. 2(a) is the periodic array structure diagram with uniformly arranged array elements, and Fig. 2 (b), (c) and (d) are the array structure diagrams of DSUE, USRE and DSRE respectively. Among them, the structure of DSUE array has been discussed in literature [11]. The existing literature data show that USRE and DSRE arrays are rarely studied.

When the number of elements in the array is fixed, the number of subarrays is inversely proportional to the number

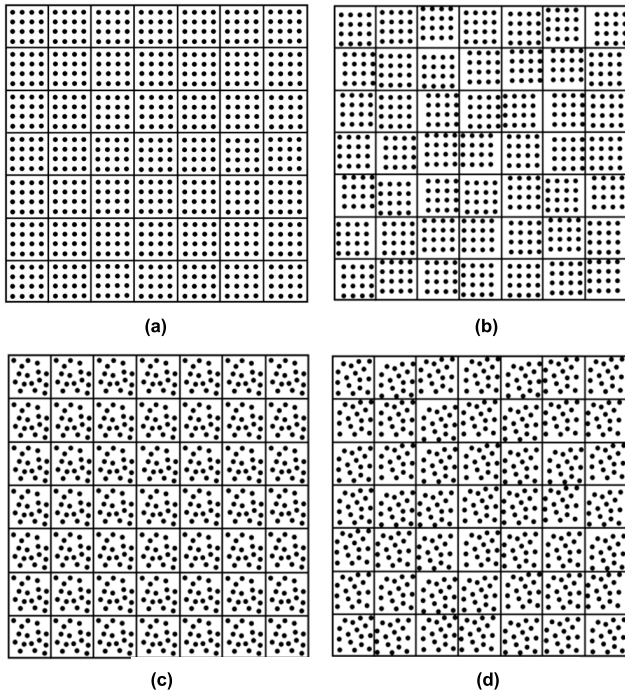


FIGURE 2. Structure diagrams of full arrays with 28×28 elements. The average array element spacing is slightly greater than one wavelength. (a) subarrays and array elements are uniform (b) DSUE (c) USRE (d) DSRE.

of elements in the subarray. For the array with 28×28 elements, it can be divided into 7×7 , 4×4 and 2×2 subarrays, and the corresponding number of elements in the subarray is 4×4 , 7×7 and 14×14 respectively. The primary purpose of this paper is to compare the PSLR characteristics of these three arrays. It is very important to ensure the same resolution (related to array aperture) of arrays with different structures. At the same time, when changing the size of subarrays, the difference between array element spacing and subarray dislocation distance should not be too large. Therefore, we make them change proportionally, as shown in the following formula, and the array apertures are the same

$$\begin{cases} k = \frac{\Delta_s 7 \times 7}{d_{4 \times 4}} = \frac{\Delta_s 4 \times 4}{d_{7 \times 7}} = \frac{\Delta_s 2 \times 2}{d_{14 \times 14}} \\ L_{a, 7 \times 7} = L_{a, 4 \times 4} = L_{a, 2 \times 2} \end{cases} \quad (1)$$

where k is the proportional constant, Δ_s is the subarray dislocation distance, L_a is the array aperture, the corresponding subscript is the number of subarrays, d is the element spacing, and its subscript is the number of elements in the subarray. For the random distribution of subarrays, the subarray length L' of different arrays is also calculated by the uniform spacing of array elements.

III. ANALYSIS METHOD

A. ARRAY SYNTHESIS USING SUBARRAYS

The total radiation pattern function of the planar array can be expressed as [15]

$$F(\theta, \varphi) = f_e(\theta, \varphi) AF_{array}(\theta, \varphi) \quad (2)$$

where $f_e(\theta, \varphi)$ is the elemental pattern and $AF_{array}(\theta, \varphi)$ is the array factor of the planar array. Because the element radiation pattern changes slowly with the angle, and the PSLR reduction level of the array radiation pattern is close to that of the array factor, only the array factor is analyzed in this paper. According to the analysis model of array structure in Fig. 1, the array factor can be expanded as follows

$$AF_{array}(\theta, \varphi) = \sum_{m,n} \sum_{m',n'} I_{mn,m'n'} e^{jk[(s_{xm}+e_{xm'})u_x + (s_{yn}+e_{yn'})u_y]} \quad (3)$$

where,

$$\begin{aligned} s_{xm} &= x_m + \Delta_{sxm} \\ s_{yn} &= y_n + \Delta_{syn} \\ e_{xm'} &= m'x_o + \Delta_{x,m'n'} \\ e_{yn'} &= n'y_o + \Delta_{y,m'n'} \\ u_x &= \sin\theta \cos\varphi - \sin\theta_o \cos\varphi_o \\ u_y &= \sin\theta \sin\varphi - \sin\theta_o \sin\varphi_o \\ u &= \sin\theta \cos\varphi, \quad v = \sin\theta \sin\varphi \end{aligned} \quad (4)$$

where mn and $m' n'$ represent the mn -th array element in the $m' n'$ -th grid. To simplify the analysis, $I_{mn,m'n'}$ is the unit excitation amplitude, and its value is 1. Δ_{sxm} and Δ_{syn} represent the dislocation distance of the subarray in the x and y directions respectively. (x_m, y_n) is the grid center coordinate. (s_{xm}, s_{yn}) represents the position of the subarray in the x and y directions, and (x_o, y_o) is the position of the uniform subarray element. $(\Delta_{x,m'n'}, \Delta_{y,m'n'})$ is the offset distance from (x_o, y_o) . $(e_{xm'}, e_{yn'})$ represents the position of the array element in the x' and y' directions in the subarray. (θ_o, φ_o) is the maximum direction of the radiation pattern.

If all subarrays in the entire array have the same structure, equation (3) can be derived as the product of two factors, as shown in equation (5)

$$\begin{aligned} AF_{array}(\theta, \varphi) &= \sum_{m,n} e^{jk[s_{xm}u_x + s_{yn}u_y]} \times \sum_{m',n'} e^{jk[e_{xm'}u_x + e_{yn'}u_y]} \\ &= AF_{ps}(\theta, \varphi) \times AF_s(\theta, \varphi) \end{aligned} \quad (5)$$

where $AF_{ps}(\theta, \varphi)$, $AF_s(\theta, \varphi)$ are the subarray position factor and subarray factor.

Then the PSLL can be calculated by

$$PSLL(\text{dB}) = 20 \log_{10} \left(\frac{AF_{sl,\max}(u, v)}{AF_{main}} \right) \quad (6)$$

where $AF_{sl,\max}(u, v)$ is the maximum sidelobe value of the radiation pattern. AF_{main} is the peak value of the main lobe.

IV. IMPROVED BAT ALGORITHM

With the improvement of computing capability, many heuristic intelligent optimization algorithms have been used to optimize complex, nonlinear, and irregular array factors, such as genetic algorithm [16], particle swarm optimization [17], firefly algorithm [18], differential evolution algorithm [19],

TABLE 1. Parameter setting of improved bat algorithm.

Parameter	Value
Maximum number of iterations	50
Population size	300
Pulse rate factor γ	0.9
frequency f	0-1
Initial Loudness A	1-2
Attenuation factor α	0.9
Flight speed v	0-0.5
Inertia weight ω	0.5-0.9
Doppler effect compensation rate C	0.1-0.9

and super multivariate optimization algorithm applied to large array optimization [20]. Bat algorithm [21], [22] is a heuristic search algorithm based on swarm intelligence, which is more suitable for solving multi-dimensional and multi-constraint optimization problems. Its good characteristics have been affirmed in the non-uniform linear array [23].

In order to analyze the array structure, we upgrade the IBA, which is proposed in our previous work [21]. This IBA is used to reduce the PSLL by optimizing the position of multiple constrained antenna array. More complicated constraints such as array spacing and array aperture will be considered in the optimization of the algorithm.

The steps and parameters of IBA are as follows:

Step1: Initialize the population and parameters. The initial population can be increased to improve the accuracy of the initial solution. On the premise that the initial position solution is reliable, the flight speed v_i of the bat should be appropriately reduced at this position. It prevents flying too fast from leaving the optimal solution range. Table 1 shows the specific parameter settings.

When the initial population is generated, it is necessary to judge the array element spacing of the initial population and modify the position of the array elements that do not meet the constraint conditions. The standard for judging the array element spacing is the minimum array element spacing $d_{min} \geq \lambda/2$, and the settings of multiple constraint conditions are as follows

$$\begin{cases} s.t \ d_{min} \leq d_{s,m'n'} - d_{s,m''n''} \leq d_{max} \\ -\Delta_s/2 \leq \Delta_{s,mn} \leq \Delta_s/2 \\ x_{a,mn} \leq L_a, \quad y_{a,mn} \leq L_a, \quad d_{a,mn} \leq 2L_a^{1/2} \end{cases} \quad (7)$$

where $\Delta_{s,mn}$ is the dislocation distance of subarray. $x_{a,mn}$, $y_{a,mn}$ indicate the constraint size of the total array in the x and y directions, $L_a = N(Md + \Delta_s)$ is the array aperture, and $d_{a,mn}$ is the spacing of elements in the array.

Under the condition of satisfying the array aperture and the array element spacing, the constraint spacing of elements in

the subarray can be expressed as

$$\begin{cases} d_{s,m'n'} - d_{s,m''n''} = \left[(x_{s,m'n'} - x_{s,m''n''})^2 + (y_{s,m'n'} - y_{s,m''n''})^2 \right]^{1/2} \\ d_{min} = \frac{\lambda}{2}, \quad d_{max} = 2L_a^{1/2} \end{cases} \quad (8)$$

where $x_{s,mn}$, $y_{s,mn}$ represent the position of elements in the subarray in the x and y directions, and $d_{s,mn}$ denotes the spacing of any two elements in the subarray.

When all array elements meet the constraint conditions, the initial population is generated and the initial solution is obtained.

Step2: Set the fitness function, substitute the initial population into the fitness function, and start iteration to generate a preliminary global optimal position solution. The fitness function is expressed as follows

$$f(A) = \min\{fitness(A)\} = \max \left\{ \frac{AF_{sl}(u, v)}{AF_{main}} \right\} \quad (9)$$

where $AF_{sl}(u, v)$ is the sidelobe area of radiation pattern, and the objective function will locate the PSLL in the whole airspace.

If a bat finds the best foraging position g_* , it will attract other bats to fly in search of food. Each bat is associated with a velocity v_i^t and a position x_i^t at iteration t . To update velocities and positions of all bats, Equations (10)–(13) are used.

$$f_i = f_{min} + (f_{max} - f_{min}) \times rand(0, 1) \quad (10)$$

$$f'_i = \frac{c + v_i^{t-1}}{c + v_g} \times f_i \times \left(1 + C_i \times \frac{g_* - x_i^{t-1}}{|g_* - x_i^{t-1}| + \varepsilon} \right) \quad (11)$$

$$v_i^t = \omega \times v_i^{t-1} + (x_i^{t-1} - g_*) \times f'_i \quad (12)$$

$$x_i^t = x_i^{t-1} + v_i^t \quad (13)$$

where f_{min} and f_{max} are the minimum and the maximum frequency. Their values are 0 and 1, respectively, depending on the specific environment. $c = 340 \text{ m/s}$ is the speed of sound in the air. C_i denotes the doppler effect compensation rate. ω is the inertia weight.

Literature [21] has shown that the adaptive local search strategy with increased Doppler effect and Doppler effect compensation rate has a good effect of increasing population diversity. This paper also introduces it to improve the performance of the algorithm.

Step3: For the local search part, once a solution is selected among the current optimal solutions, a new solution is generated using a random walk

$$x_{new} = x_{old} + N[0, 1] \times A^t \quad (14)$$

where A^t is the average loudness of all bats. The new solution should also meet the constraint conditions.

Step4: The fitness function is used to evaluate the local new solution. When the new solution is better than the current

optimal solution, the loudness and pulse emission rate are updated by the following equations

$$A_i^{t+1} = \alpha A_i^t \tag{15}$$

$$r_i^{t+1} = r_i^0 [1 - \exp(-\gamma t)] \tag{16}$$

where α and γ are attenuation factor and pulse rate factor. The initial loudness A_i can be [1] and [2], while the initial emission rate r_i^0 can be [0,1].

Step5: Update the current global optimal solution. If the loop reaches the maximum number of iterations, the optimal solution and the optimal fitness function value are output. If not, it returns to step2 to continue the iteration.

A. REDUNDANCY THEORY

The minimum redundant array (MRA) is widely used in microwave radiometer [24], [25], radio astronomy [26], adaptive beamforming [27] and MIMO radar [28]. Any antenna pair in the array will form a baseline vector, and redundancy means that the baseline vectors are the same. The process of searching for MRA is to find the array structure with minimum redundancy.

Theoretically, a planar array with N elements can have up to $N(N-1)$ non-redundant baselines. However, the actual number of non-redundant baselines is usually less than this value because the planar array elements are difficult to be completely random. Generally, the redundancy of an array is measured by R , which is defined as the ratio of the ideal number of non-redundant baselines $S_{id} = N(N-1)$ to the actual number of non-redundant baselines S_{re} .

The randomness of array element arrangement in aperiodic array is closely related to the PLSR effect. The redundancy can represent the uniformity of the array, and we can infer that the redundancy of the array can reflect its PSLR effect to some extent. It is not a mature theory to reduce PSLR by optimizing array redundancy, but the close mapping relationship between redundancy and aperiodic arrays with different uniformity can be seen through simulation in this paper.

V. SIMULATION RESULTS AND ANALYSIS

A. THREE KINDS OF ARRAYS PSLR CHARACTERISTIC

In order to simplify the analysis, we take arrays with 12×12 , 18×18 and 28×28 elements as examples. Three kinds of subarrays can be found for each case. For example, an array with 28×28 elements can be divided into 2×2 , 4×4 and 7×7 subarrays. The following analysis methods and conclusions can generally be extended to other similar arrays with different numbers of array elements.

For all arrays in this paper, the positions of array elements are optimized by IBA at the frequency of 10 GHz. The average spacing of array elements is $d_{ave} \geq \lambda$. Fig. 3(a) is the comparison diagram of PSLR effect of three arrays which have 6×6 (array elements 12×12), 6×6 (array elements 18×18) and 7×7 (array elements 28×28) subarrays. The dislocation distance between these subarrays is $\Delta_s = 0.87\lambda$.

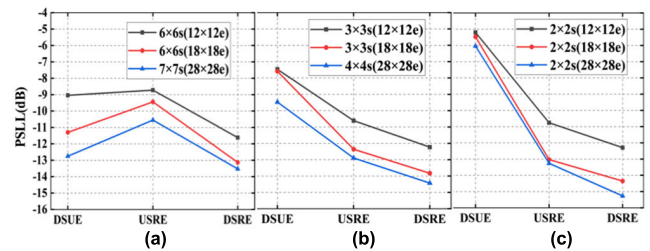


FIGURE 3. The PSLR effect of three arrays with different number of elements when the number of subarrays is (a) large; (b) moderate; (c) small. The s represents the number of subarrays. The e represents the number of elements in the array.

When the number of subarrays is large, the PSLR effect of DSUE arrays is better than that of USRE arrays. This is because the dislocations of DSUE arrays have more non-uniformity than the randomness of USRE arrays when the number of elements in subarrays is relatively small. DSRE arrays can greatly break the periodicity of arrays, and their PSLR effect is superior to other arrays.

Fig. 3(b) and Fig. 3(c) illustrate the PSLR effect of three arrays when the numbers of subarrays are moderate and small, respectively. In order to ensure the same array aperture for the same number of array elements, the relationship between dislocation distance and element spacing should satisfy equation (1). In the case of 28×28 elements, the dislocation distances are $\Delta_{s,4 \times 4} = 0.93\lambda$ and $\Delta_{s,2 \times 2} = 0.99\lambda$, respectively. When the numbers of subarrays are less than the numbers of elements in the corresponding subarrays, the PSLR effect of USRE arrays is better than that of DSUE arrays, and that of DSRE arrays is still the best.

Fig. 4 shows the two-dimensional radiation patterns of the array structures corresponding to Fig. 2 sequentially. As shown in Fig. 4(a), the GL has the same amplitude as the main lobe. The peak sidelobe levels (PSLLs) and positions are also indicated in the radiation patterns. It can be clearly seen that due to the non-uniform arrangement of array elements, the peak sidelobe positions are distributed in the visible range of the entire airspace.

The corresponding relationship between PSLL and redundancy of arrays with different number of array elements is shown in Tables 2, 3 and 4. As can be seen from these tables, the three kinds of aperiodic arrays with different subarray divisions have different non-uniformity. The array structure with high degree of non-uniformity has less redundancy. Redundancy can effectively reflect the non-uniformity of arrays, which is helpful for researchers to grasp the randomness of arrays in the design process.

In literature [14], the array with rotating subarrays composed of 144 elements is optimized by traditional genetic algorithm (GA) at the frequency of 10 GHz. To highlight the proficiency of IBA, particle swarm optimization (PSO) is also selected to optimize DSRE $_{4 \times 4}$ array with 12×12 elements. The initial population number is set to 200. When the average relative change in fitness function values over 10 generations is less than 1×10^{-4} , the optimization process is terminated. The optimization results of IBA are obtained

TABLE 2. Correspondence between PSLL and redundancy of arrays with 12×12 elements.

Number of array elements	12×12								
Number of subarrays	2×2			3×3			4×4		
Array structure	DSRE	USRE	DSUE	DSRE	USRE	DSUE	DSRE	USRE	DSUE
PSLL (dB)	-12.29	-10.76	-5.20	-12.23	-10.61	-7.47	-11.62	-8.72	-9.04
Number of non-redundant baselines	18616	15114	4758	18326	10008	5252	18044	5682	6998
Redundancy (<i>R</i>)	1.11	1.36	4.33	1.12	2.06	3.92	1.14	3.62	2.94

TABLE 3. Correspondence between PSLL and redundancy of arrays with 18×18 elements.

Number of array elements	18×18								
Number of subarrays	2×2			3×3			6×6		
Array structure	DSRE	USRE	DSUE	DSRE	USRE	DSUE	DSRE	USRE	DSUE
PSLL (dB)	-14.35	-13.03	-5.47	-13.83	-12.36	-7.35	-13.13	-9.44	-11.30
Number of non-redundant baselines	96938	79844	12854	96848	52518	13748	95222	24678	40624
Redundancy (<i>R</i>)	1.08	1.31	8.14	1.08	1.99	7.61	1.10	4.24	2.58

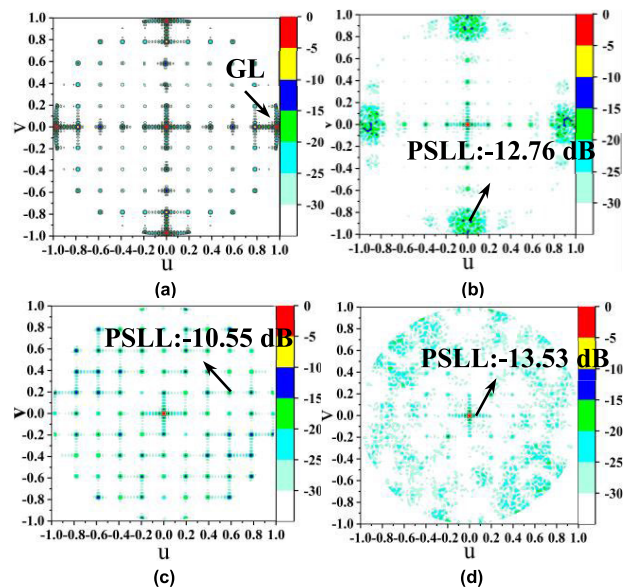


FIGURE 4. Two-dimensional radiation patterns corresponding to the array structure diagrams of Fig. 2. (a) subarrays and array elements are uniform (b) DSUE (c) USRE (d) DSRE.

when $\nu = 0.4$, $\omega = 0.75$. The PSO optimization results are calculated when the inertia constant $\omega = 0.7$, the acceleration constant $c_1 = c_2 = 1.5$ and the maximum particle velocity $V_{max} = 0.12$. As shown in Fig. 5(a), the convergence curves of these two algorithms are compared with those of GA applied to tiled array in literature [14]. It can be seen that IBA is superior to the other two algorithms in terms of convergence speed and accuracy. In this paper, IBA is calculated by Intel core i7 8700 processor. Compared with literature [14], the calculation time of IBA over element number is shorter, as shown in Fig. 5(b), which is closely related to the number of iterations and convergence characteristics of the algorithm.

As shown in Table 2, the PSL of DSRE arrays with 12×12 elements worsen as the number of subarrays increases. The array length in literature [14] is 8λ , and the average array spacing is less than 1λ . The results show that the PSL is

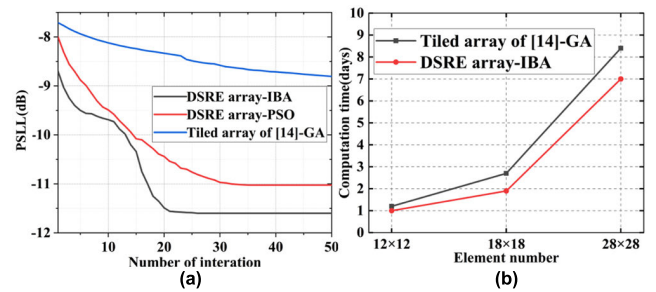


FIGURE 5. Optimization results for array antennas with 12×12 elements. (a) Convergence curves over iteration for IBA in this paper, traditional PSO and GA in literature [14]. (b) Comparison of calculation time over element number for IBA in this paper and GA in literature [14].

about -11 dB. In this paper, in the case of the array length greater than 8λ and the average array spacing slightly greater than 1λ , the worst PSL is -11.62 dB, which is the result of PSLR with the largest number of subarrays (4×4). When the number of subarrays is 2×2 , the PSL can be suppressed to -12.29 dB. This is obviously superior to the subarray rotation structure proposed in literature [14].

As the number of array elements increases, the optimization time does not increase linearly, which depends on the accuracy of the initial population location of the algorithm. Once the population is located near the optimal position, the fitness function will converge rapidly, thus shortening the optimization time. According to the subarray division scheme, the optimization of array elements arrangement in each subarray only needs to be calculated once, and the dislocation optimization of all subarrays needs to be considered. Thus, the number of design variables is less than that of completely random arrays. Therefore, no matter the optimization time or the number of design variables, the DSRE array has low computational complexity.

In summary, the PSLR effect of DSUE and USRE arrays varies with the number of subarrays. No matter for which array structure, DSRE array is the best choice in the array design with higher requirements for PSLR, even for a small number of random elements in the subarray. Compared with

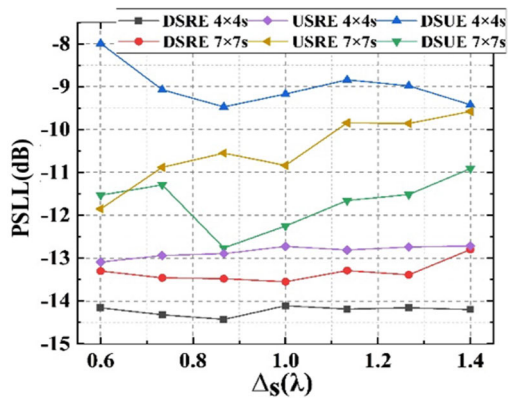


FIGURE 6. Influence of subarray dislocation distance on PSLs.

other aperiodic arrays, such as subarray rotating random array, DSRE array also has good performance.

B. INFLUENCE OF SUBARRAY DISLOCATION DISTANCE ON PSLR

It is very important to select the optimal dislocation distance of subarrays to improve the performance of array antennas in the subarray level aperiodic array. This section will mainly study the influence of dislocation distance on the PSLR effect. The array with 28×28 elements is still considered. From the perspective of engineering application, there are too many randomly arranged elements in the 2×2 subarrays, and the design of a single subarray is relatively complex and has low application value. So, it will not be analyzed here. This section discusses the PSLR effect of three kind of array structures under different dislocation distances with 7×7 and 4×4 subarrays.

In Fig. 6, the subarray dislocation distance is $0.6\lambda \leq \Delta_s \leq 1.4\lambda$. The array aperture is the same under the same subarray dislocation distance. The average array element spacing is no longer proportional to the subarray dislocation distance, but is determined by the array aperture.

According to the overall trend in Fig. 6, the PSLR effect is $DSRE_{4 \times 4} > DSRE_{7 \times 7} > USRE_{4 \times 4} > DSUE_{7 \times 7} > USRE_{7 \times 7} > DSUE_{4 \times 4}$. For the proposed structures, the PSLR effect is the best when the subarray dislocation distance is slightly less than a wavelength or the average array element spacing.

The PSLs of $DSRE_{4 \times 4}$, $DSRE_{7 \times 7}$ and $USRE_{4 \times 4}$ arrays show a stable trend with the increase of Δ_s . As shown in Table 4, the redundancy of these three arrays increases gradually. From the analysis of array structures, the non-uniformity of $DSRE_{4 \times 4}$ and $DSRE_{7 \times 7}$ arrays are affected by subarray dislocation and the non-uniform arrangement of array elements, with the latter being the dominant factor affecting the non-uniformity of array. Therefore, the more the array elements are arranged non-uniformly, the stronger the PSLR ability becomes. For $USRE_{4 \times 4}$ and $DSUE_{7 \times 7}$, the former has 7×7 non-uniformly arranged array elements, while the latter has 7×7 dislocated subarrays. The number of non-uniform influencing factors is the same, but the PSLR ability of the

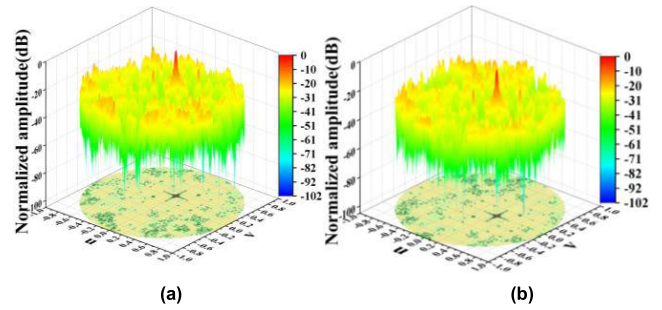


FIGURE 7. 3D scanning patterns and plane maps of DSRE array with 7×7 subarrays (a) $u = 15^\circ$ (b) $v = 15^\circ$.

former is better than that of the latter. The reason is that the non-uniform arrangement of array elements plays a main role in influencing the non-uniformity of array. The same is true for $USRE_{7 \times 7}$ and $DSUE_{4 \times 4}$. When the number of single non-uniform influencing factors is different, such as $USRE_{7 \times 7}$ and $DSUE_{7 \times 7}$, the former has 4×4 non-uniformly arranged array elements, and the latter has 7×7 dislocated subarrays. In this case, the larger number of dislocated subarrays dominate the non-uniformity of the array, so the PSLR effect of the latter is better than that of the former.

The PSLR effect of all array structures in Fig. 6 basically weaken with the increase of Δ_s , especially $USRE_{7 \times 7}$ and $DSUE_{7 \times 7}$. For arrays with a single non-uniform factor, it will inevitably lead to the increase of the subarrays spacing and the elements spacing with the increase of Δ_s . The increase of either of them will worsen the PSL of the array pattern. We can see that $DSUE_{4 \times 4}$ has a different change rule. The reason is that the number of dislocated subarrays is quite small, which is the only factor affecting the non-uniformity of the array. This results in its unspecific variation rule with Δ_s .

C. SCAN OF ARRAY

The scanning characteristic is an important index to evaluate the performance of array antenna. The phased array antenna with wide-angle scanning capability is widely used in radar, direction finding and remote sensing. This section will further verify the wide scanning characteristic of the array structures proposed in this paper.

For the array antenna with 28×28 elements, Fig. 7 is the full-space three-dimensional scanning patterns and plane maps of DSRE array with 7×7 subarrays when scanning angles are 15° in the u axis and 15° in the v axis. For a small scanning angle of 15° , the PSL of the array radiation pattern is below -13.5 dB, and the SLL does not increase obviously. Fig. 8 shows the full-space three-dimensional scanning patterns and plane maps of DSUE array and USRE array with 7×7 subarrays when scanning angles are 15° in the u axis and 15° in the v axis. The u -axis and the v -axis can refer to the labels in Fig. 7. Table 5 lists the corresponding PSL values in Fig. 7 and 8. Compared with the radiation pattern of DSRE array, it can be found that the scanning characteristics of DSUE array and USRE array are poor

TABLE 4. Correspondence between PSLL and redundancy of arrays with 28x28 elements.

Number of array elements	28x28								
	2x2			4x4			7x7		
Number of subarrays									
Array structure	DSRE	USRE	DSUE	DSRE	USRE	DSUE	DSRE	USRE	DSUE
PSLL (dB)	-15.27	-13.26	-6.04	-14.43	-12.89	-9.47	-13.53	-10.55	-12.76
Number of non-redundant baselines	607620	460218	42574	584884	250328	83726	576616	118748	212452
Redundancy (R)	1.01	1.33	14.42	1.05	2.45	7.33	1.06	5.17	2.89

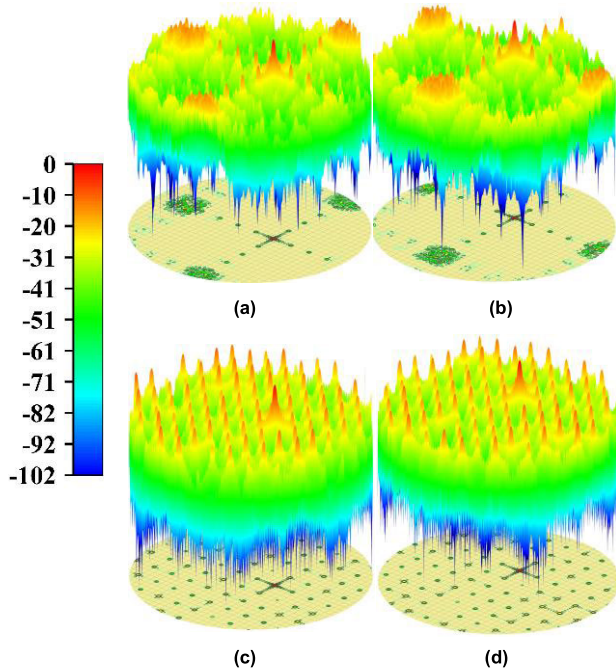


FIGURE 8. 3D scanning patterns and plane maps of DSUE array and USRE array with 7x7 subarrays (a) DSUE, $u = 15^\circ$ (b) DSUE, $v = 15^\circ$ (c) USRE, $u = 15^\circ$ (d) USRE, $v = 15^\circ$.

TABLE 5. PSLL of three arrays for different scanning angles.

Array structure	DSRE		DSUE		USRE	
Scanning angles in u axis	15°	0°	15°	0°	15°	0°
Scanning angles in v axis	0°	15°	0°	15°	0°	15°
PSLL (dB)	-13.51	-13.50	-12.75	-12.74	-8.88	-8.87

even at small scanning angles. With the increase of the scanning angle, the scanning characteristics are even worse, because the radiation energy is concentrated in some fixed areas, resulting in the increase of PSLL. However, due to the high non-uniformity of array elements, DSRE array can effectively disperse the radiation energy, and thus reduce the PSLL.

For a larger scanning range, DSRE array can also maintain good radiation characteristics. Fig. 9 shows the scanning patterns and plane maps at 30° and 60° in u axis and v axis respectively. And their PSLL values are shown in Table 6. It can be seen from the figure that at larger scanning angles of 30° and 60° , the PSLL and the average SLL do not increase significantly with the increase of scanning angle.

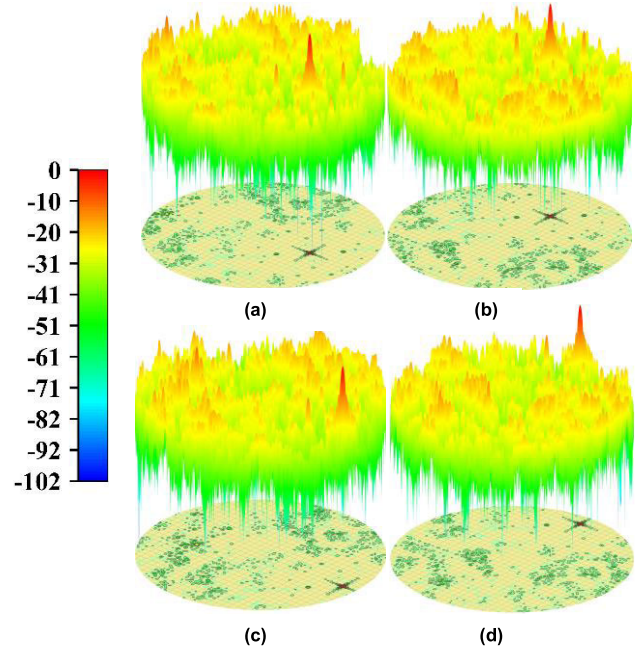


FIGURE 9. The 3D radiation patterns and plane maps of DSRE array with 7x7 subarrays scanned at 30° and 60° in the u and v axis. (a) $u = 30^\circ$ (b) $v = 30^\circ$ (c) $u = 60^\circ$ (d) $v = 60^\circ$.

TABLE 6. PSLL of DSRE array for different scanning angles.

Array structure	DSRE			
Scanning angles in u axis	30°	0°	60°	0°
Scanning angles in v axis	0°	30°	0°	60°
PSLL (dB)	-13.45	-13.43	-13.05	-13.04

TABLE 7. PSLL of 7x7 subarrays for different frequencies.

Frequency (GHz)	6.12	8.11	10.00	12.00	14.29	15.79	17.65
PSLL(dB) 7x7s DSUE	-7.17	-12.94	-12.76	-12.72	-9.74	-9.71	-9.82
PSLL(dB) 7x7s USRE	-5.24	-10.49	-10.55	-8.88	-7.66	-5.25	-5.14
PSLL(dB) 7x7s DSRE	-7.28	-13.51	-13.53	-13.49	-10.12	-10.14	-10.13

D. FREQUENCY CHARACTERISTIC

Aperiodic array antennas have very stable modes over a wide frequency range, making them very suitable for operation in large bandwidths. This section will analyze the PSLL effect of three array structures at different frequencies and provide some design suggestions.

TABLE 8. PSLR of 4×4 subarrays for different frequencies.

Frequency (GHz)	6.12	8.11	10.00	12.00	14.29	15.79	17.65
PSLL(dB) 4×4s DSUE	-7.04	-12.56	-9.47	-9.51	-6.05	-5.97	-6.14
PSLL(dB) 4×4s USRE	-7.18	-12.90	-12.89	-9.74	-9.77	-9.81	-9.87
PSLL(dB) 4×4s DSRE	-7.21	-14.32	-14.43	-14.34	-14.42	-14.54	-14.39

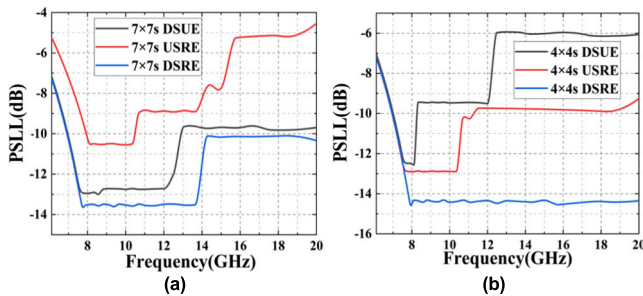
**FIGURE 10.** The PSLL effect of three structures with 28×28 elements in the frequency range (6GHz-20GHz). (a) 7×7 subarrays (b) 4×4 subarrays.

Fig. 10 shows the PSLL effect varying with frequency for 28×28 elements with 7×7 and 4×4 subarrays respectively. The array structures are optimized at the frequency of 10 GHz. Table 7 and 8 show the PSLL values at different frequencies in Fig. 10 (a) and (b). From the perspective of the PSLL effect, the PSLL of the three arrays in Fig. 10 (a) are stable at low frequency band, and mutate at high frequency band. The lobe levels of DSUE array and DSRE array tend to be stable at high frequency, while the lobe levels of USRE array rise sharply with increasing frequency. This is because the adaptive frequency width of the arrays is related to their non-uniformity. The higher the non-uniformity of aperiodic array is, the more stable its radiation pattern is over a wider frequency range, and the PSLL mutation is reduced. The PSLL of the three array structures in Fig. 10 (b) show similar frequency characteristics as those in Fig. 10 (a). The PSLLs of DSUE array with 4×4 subarrays and USRE array with 7×7 subarrays show a similar tendency as the frequency increases, while the curves of USRE array with 4×4 subarrays and DSUE array with 7×7 subarrays look similar. It is worth mentioning that the PSLL ability of DSRE array with 4×4 subarrays remain stable with the increase of frequency. The PSLL begins to increase at the frequency of 27 GHz which is beyond the frequency range shown in the figure. So, it can be seen that the adaptive frequency width of DSRE array with 4×4 subarrays is very wide. It also has been shown in Fig. 6 that this array has the best PSLL effect. For the arrays proposed in this paper, the higher the non-uniformity of the array, the wider the adaptive frequency width.

VI. CONCLUSION

In this paper, three aperiodic arrangement methods of subarray-level rectangular grid array antennas are proposed. The IBA is used to optimize array structures through the dislocation position of subarrays and random position of

elements in the subarray. The PSLL effect of three kinds of arrays with different number of elements and subarrays are analyzed, and the non-uniformity of arrays are characterized by their redundancy. The results show that the PSLL effect of DSRE arrays is better than those of DSUE arrays and USRE arrays. The array with 28×28 elements is taken as an example to study the PSLL in terms of dislocation distance of subarray, scanning angle and applicable frequency. The dislocation distance of subarrays slightly less than one wavelength is the best choice. The DSRE arrays can maintain good PSLL ability at the large scanning angle of up to 60° , which also have wider adaptive frequency width. The proposed design method of DSRE array is a universal and scalable method. For example, the array with 28×28 elements can be treated as a new subarray to further expand the scale of aperiodic array antenna. By inducing the rotation degree of freedom, such as subarray rotation or Fermat spiral, we can combine rotation, dislocation and random elements approaches to study the RSLR effect. This is of great value to the design and application of large-scale aperiodic array antennas.

REFERENCES

- [1] S. Caorsi, A. Lommi, A. Massa, and M. Pastorino, "Peak sidelobe level reduction with a hybrid approach based on GAs and difference sets," *IEEE Trans. Antennas Propag.*, vol. 52, no. 4, pp. 1116–1121, Apr. 2004.
- [2] A. B. Smolders and H. J. Visser, "Low side-lobe circularly-polarized phased arrays using a random sequential rotation technique," *IEEE Trans. Antennas Propag.*, vol. 62, no. 12, pp. 6476–6481, Dec. 2014.
- [3] L. H. Gabrielli and H. E. Hernandez-Figueroa, "Aperiodic antenna array for secondary lobe suppression," *IEEE Photon. Technol. Lett.*, vol. 28, no. 2, pp. 209–212, Jan. 19, 2016.
- [4] T. G. Spence and D. H. Werner, "Design of broadband planar arrays based on the optimization of aperiodic tilings," *IEEE Trans. Antennas Propag.*, vol. 56, no. 1, pp. 76–86, Jan. 2008.
- [5] R. L. Haupt, "Thinned arrays using genetic algorithms," *IEEE Trans. Antennas Propag.*, vol. 42, no. 7, pp. 993–999, Jul. 1994.
- [6] H. Malik, J. Burki, and M. Z. Mumtaz, "Adaptive pulse compression for sidelobes reduction in stretch processing based MIMO radars," *IEEE Access*, vol. 10, pp. 93231–93244, 2022.
- [7] E. Ghayoula, A. Bouallegue, R. Ghayoula, J. Fattahi, E. Pricop, and J. Chouinard, "Radiation pattern synthesis using hybrid Fourier-Woodward-Lawson-neural networks for reliable MIMO antenna systems," in *Proc. IEEE Int. Conf. Syst., Man, Cybern. (SMC)*, Oct. 2017, pp. 3290–3295.
- [8] J. Dong, Q. Li, F. He, W. Ni, and Y. Zhu, "Co-array properties of minimum redundancy linear arrays with minimum sidelobe level," in *Proc. 8th Int. Symp. Antennas, Propag. EM Theory*, Nov. 2008, pp. 74–77.
- [9] M. Moebus and A. M. Zoubir, "2D nonuniform array design for imaging applications," in *Proc. Int. ITG Workshop Smart Antennas*, Feb. 2008, pp. 180–183.
- [10] M. Karaman, I. O. Wygant, Ö. Oralkan, and B. T. Khuri-Yakub, "Minimally redundant 2-D array designs for 3-D medical ultrasound imaging," *IEEE Trans. Med. Imag.*, vol. 28, no. 7, pp. 1051–1061, Jul. 2009.
- [11] Y. V. Krivosheev, A. V. Shishlov, and V. V. Denisenko, "Grating lobe suppression in aperiodic phased array antennas composed of periodic subarrays with large element spacing," *IEEE Antennas Propag. Mag.*, vol. 57, no. 1, pp. 76–85, Feb. 2015.
- [12] H. Wang, D.-G. Fang, and Y. Leonard Chow, "Grating lobe reduction in a phased array of limited scanning," *IEEE Trans. Antennas Propag.*, vol. 56, no. 6, pp. 1581–1586, Jun. 2008.
- [13] K. C. Kerby and J. T. Bernhard, "Sidelobe level and wideband behavior of arrays of random subarrays," *IEEE Trans. Antennas Propag.*, vol. 54, no. 8, pp. 2253–2262, Aug. 2006.

- [14] J. Diao, J. W. Kunzler, and K. F. Warnick, "Sidelobe level and aperture efficiency optimization for tiled aperiodic array antennas," *IEEE Trans. Antennas Propag.*, vol. 65, no. 12, pp. 7083–7090, Dec. 2017.
- [15] T. J. Brockett and Y. Rahmat-Samii, "Subarray design diagnostics for the suppression of undesirable grating lobes," *IEEE Trans. Antennas Propag.*, vol. 60, no. 3, pp. 1373–1380, Mar. 2012.
- [16] K. Chen, X. Yun, Z. He, and C. Han, "Synthesis of sparse planar arrays using modified real genetic algorithm," *IEEE Trans. Antennas Propag.*, vol. 55, no. 4, pp. 1067–1073, Apr. 2007.
- [17] R. M. Maina, P. Kibet Lang'at, and P. K. Kihato, "Collaborative beamforming in wireless sensor networks using a novel particle swarm optimization algorithm variant," *Heliyon*, vol. 7, no. 10, Oct. 2021, Art. no. e08247.
- [18] P. Baumgartner, T. Bauernfeind, O. Bíró, A. Hackl, C. Magele, W. Renhart, and R. Torchio, "Multi-objective optimization of Yagi-Uda antenna applying enhanced firefly algorithm with adaptive cost function," *IEEE Trans. Magn.*, vol. 54, no. 3, pp. 1–4, Mar. 2018.
- [19] H. Liu, H. Zhao, W. Li, and B. Liu, "Synthesis of sparse planar arrays using matrix mapping and differential evolution," *IEEE Antennas Wireless Propag. Lett.*, vol. 15, pp. 1905–1908, 2016.
- [20] X. Xu, C. Liao, L. Zhou, and F. Peng, "Grating lobe suppression of non-uniform arrays based on position gradient and sigmoid function," *IEEE Access*, vol. 7, pp. 106407–106416, 2019.
- [21] Y. Pan and J. Zhang, "Synthesis of linear symmetric antenna arrays using improved bat algorithm," *Microw. Opt. Technol. Lett.*, vol. 62, no. 6, pp. 2383–2389, Jun. 2020.
- [22] B. Chen, J. Yang, H. Zhang, and M. Yang, "An improved spherical vector and truncated mean stabilization based bat algorithm for UAV path planning," *IEEE Access*, vol. 11, pp. 2396–2409, 2023.
- [23] A. Das, D. Mandal, S. P. Ghoshal, and R. Kar, "An efficient side lobe reduction technique considering mutual coupling effect in linear array antenna using BAT algorithm," *Swarm Evol. Comput.*, vol. 35, pp. 26–40, Aug. 2017.
- [24] T. Zheng, F. Hu, L. Wu, J. Su, and H. Hu, "Synthesis of large alias-free field-of-view linear arrays for synthetic aperture interferometric radiometers," *IEEE Trans. Antennas Propag.*, vol. 68, no. 12, pp. 7916–7926, Dec. 2020.
- [25] J. Dong, Q. Li, R. Jin, Y. Zhu, Q. Huang, and L. Gui, "A method for seeking low-redundancy large linear arrays in aperture synthesis microwave radiometers," *IEEE Trans. Antennas Propag.*, vol. 58, no. 6, pp. 1913–1921, Jun. 2010.
- [26] J. Zhang, R. Ansari, X. Chen, J. Campagne, C. Magneville, and F. Wu, "Sky reconstruction from transit visibilities: PAON-4 and Tianlai dish array," *Monthly Notices Roy. Astronomical Soc.*, vol. 461, no. 2, pp. 1950–1966, May 2016.
- [27] C.-Y. Tseng and L. J. Griffiths, "Sidelobe suppression in minimum redundancy linear arrays," in *Proc. IEEE 6th SP Workshop Stat. Signal Array Process.*, Oct. 1992, pp. 288–291.
- [28] J. Dong, Q. Li, and W. Guo, "A combinatorial method for antenna array design in minimum redundancy MIMO radars," *IEEE Antennas Wireless Propag. Lett.*, vol. 8, pp. 1150–1153, 2009.



HONGTAO ZHANG was born in Shandong, Linyi, China, in 1998. He is currently pursuing the master's degree with Shanxi University. His research interest includes the synthesis of planar arrays.



XUELEI CHEN received the Ph.D. degrees from the Physics Department, Columbia University, in 1999. He was a Postdoctoral Fellow with the Physics Department, The Ohio State University, and the Institute of Theoretical Physics, University of California at Santa Barbara, Santa Barbara. He joined National Astronomical Observatory, in 2004. He mainly engaged in theoretical research and data analysis in cosmology and particle astrophysics. His research interests include galaxy formation, especially the formation of the first generation of luminous objects in the universe, reionization, and their 21 cm observations.



FENGQUAN WU received the Ph.D. degree in theoretical physics from the Institute of High Energy Physics, Beijing, China, in 2007. Then, he joined National Astronomical Observatory, where he worked on the CMB perturbation theory, large scale structure survey, and radio astronomy. His current research interests include interferometer array, 21 cm radio detection, FRB, transient radio source detection, and 21 cm global spectrum detection.



YUFENG LIU was born in Shanxi, Lüliang, China, in 1986. He received the Ph.D. degree in radio physics from Sichuan University, Sichuan, China, in 2014. In 2015, he joined the School of Physics and Electronic Engineering, Shanxi University. His research interests include computational electromagnetics and antenna design.



WENMEI ZHANG (Senior Member, IEEE) received the B.S. and M.S. degrees in electronic engineering from the Nanjing University of Science and Technology, Nanjing, China, in 1992 and 1995, respectively, and the Ph.D. degree in electronic engineering from Shanghai Jiao Tong University, Shanghai, China, in 2004. Currently, she is a Professor with the School of Physics and Electronic Engineering, Shanxi University, Taiyuan, China. Her research interests include microwave and millimeter-wave integrated circuits, EMC, and microstrip antenna.



JIAO ZHANG received the dual Ph.D. degree from the University of Chinese Academy of Sciences and Université Paris-Sud, in 2017. Currently, she is a Lecturer with the School of Physics and Electronic Engineering, Shanxi University, Taiyuan, China. Her current research interests include array signal processing and communication signal processing.